

## Discovery and Characterization of an Eccentric, Warm Saturn Transiting the Solar Analog TOI-4994\*

ROMY RODRÍGUEZ MARTÍNEZ <sup>1</sup>, JASON D. EASTMAN <sup>1</sup>, KAREN A. COLLINS <sup>1</sup>, JOSEPH E. RODRIGUEZ <sup>2</sup>,  
DAVID CHARBONNEAU <sup>1</sup>, SAMUEL N. QUINN <sup>1</sup>, DAVID W. LATHAM <sup>1</sup>, CARL ZIEGLER <sup>3</sup>, RAFAEL BRAHM <sup>4,5</sup>,  
TYLER R. FAIRNINGTON <sup>6</sup>, SOLÈNE ULMER-MOLL <sup>6,8</sup>, KEIVAN G. STASSUN <sup>9</sup>, OLGA SUAREZ <sup>10</sup>,  
TRISTAN GUILLOT <sup>10</sup>, MELISSA J. HOBSON <sup>7</sup>, JOSHUA N. WINN <sup>11</sup>, SHUBHAM KANODIA <sup>12</sup>, MARTIN SCHLECKER <sup>13</sup>,  
R.P. BUTLER <sup>12</sup>, JEFFREY D. CRANE <sup>12</sup>, STEVE SHECTMAN <sup>12</sup>, JOHANNA K. TESKE <sup>12</sup>, DAVID OSIP <sup>12</sup>,  
YURI BELETSKY <sup>12</sup>, MATTHEW P. BATTLE <sup>7</sup>, ANGELICA PSARIDI <sup>7</sup>, PEDRO FIGUEIRA <sup>7</sup>, MONIKA LENDL <sup>7</sup>,  
FRANÇOIS BOUCHY <sup>7</sup>, STÉPHANE UDRY <sup>7</sup>, MICHELLE KUNIMOTO <sup>14</sup>, DJAMEL MÉKARNIA <sup>10</sup>, LYU ABE <sup>10</sup>,  
TRIFON TRIFONOV <sup>15,16,17</sup>, MARCELO TALA PINTO <sup>4,5</sup>, JAN EBERHARDT <sup>15</sup>, NESTOR ESPINOZA <sup>18</sup>,  
THOMAS HENNING <sup>17</sup>, ANDRÉS JORDÁN <sup>4</sup>, FELIPE I. ROJAS <sup>19</sup>, KHALID BARKAOUI <sup>20,21,22</sup>, HOWARD M. RELLES <sup>1</sup>,  
GREGOR SRDOC <sup>23</sup>, KEVIN I. COLLINS <sup>24</sup>, SARA SEAGER <sup>25,26,27</sup>, AVI SHPORER <sup>14</sup>, MICHAEL VEZIE <sup>25</sup>,  
CHRISTINA HEDGES <sup>28</sup> AND ISMAEL MIRELES <sup>29</sup>

<sup>1</sup>Center for Astrophysics | Harvard & Smithsonian, 60 Garden St, Cambridge, MA 02138, USA

<sup>2</sup>Center for Data Intensive and Time Domain Astronomy, Department of Physics and Astronomy, Michigan State University, East Lansing, MI 48824, USA

<sup>3</sup>Department of Physics, Engineering and Astronomy, Stephen F. Austin State University, 1936 North St, Nacogdoches, TX 75962, USA

<sup>4</sup>Facultad de Ingeniera y Ciencias, Universidad Adolfo Ibáñez, Av. Diagonal las Torres 2640, Peñalolén, Santiago, Chile

<sup>5</sup>Millennium Institute for Astrophysics, Chile

<sup>6</sup>Centre for Astrophysics, University of Southern Queensland, West Street, Toowoomba, QLD 4350, Australia

<sup>7</sup>Observatoire astronomique de l'Université de Genève, 51 Chemin Pegasi, 1290 Versoix, Switzerland

<sup>8</sup>Physikalisches Institut, University of Bern, Gesellschaftsstrasse 6, 3012 Bern, Switzerland

<sup>9</sup>Department of Physics and Astronomy, Vanderbilt University, Nashville, TN 37235, USA

<sup>10</sup>Université Côte d'Azur, Observatoire de la Côte d'Azur, CNRS, Laboratoire Lagrange, Bd de l'Observatoire, CS 34229, 06304 Nice cedex 4, France

<sup>11</sup>Department of Astrophysical Sciences, Princeton University, Princeton, NJ 08544, USA

<sup>12</sup>Carnegie Science Earth and Planets Laboratory, 5241 Broad Branch Road, NW, Washington, DC 20015, USA

<sup>13</sup>Department of Astronomy and Steward Observatory, University of Arizona, Tucson, AZ 85721, USA

<sup>14</sup>Department of Physics and Kavli Institute for Astrophysics and Space Research, Massachusetts Institute of Technology, 77 Massachusetts Avenue, Cambridge, MA 02139, USA

<sup>15</sup>Max-Planck-Institut für Astronomie, Königstuhl 17, D-69117 Heidelberg, Germany

<sup>16</sup>Department of Astronomy, Sofia University "St Kliment Ohridski", 5 James Bourchier Blvd, BG-1164 Sofia, Bulgaria

<sup>17</sup>Landessternwarte, Zentrum für Astronomie der Universität Heidelberg, Königstuhl 12, D-69117 Heidelberg, Germany

<sup>18</sup>Space Telescope Science Institute, Baltimore, MD 21218, USA

<sup>19</sup>Instituto de Astrofísica, Facultad de Física, Pontificia Universidad Católica de Chile, Av. Vicuña Mackenna 4860, Santiago, Chile.

<sup>20</sup>Astrobiology Research Unit, Université de Liège, 19C Allée du 6 Août, 4000 Liège, Belgium

<sup>21</sup>Department of Earth, Atmospheric and Planetary Science, Massachusetts Institute of Technology, 77 Massachusetts Avenue, Cambridge, MA 02139, USA

<sup>22</sup>Instituto de Astrofísica de Canarias (IAC), Calle Vía Láctea s/n, 38200, La Laguna, Tenerife, Spain

<sup>23</sup>Kotizarovci Observatory, Sarsoni 90, 51216 Viskovo, Croatia

<sup>24</sup>George Mason University, 4400 University Drive, Fairfax, VA, 22030 USA

<sup>25</sup>Department of Physics and Kavli Institute for Astrophysics and Space Research, Massachusetts Institute of Technology, Cambridge, MA 02139, USA

<sup>26</sup>Department of Earth, Atmospheric and Planetary Sciences, Massachusetts Institute of Technology, Cambridge, MA 02139, USA

<sup>27</sup>Department of Aeronautics and Astronautics, MIT, 77 Massachusetts Avenue, Cambridge, MA 02139, USA

<sup>28</sup>NASA Goddard Space Flight Center, 8800 Greenbelt Rd, Greenbelt, MD 20771, USA

<sup>29</sup>Department of Physics and Astronomy, University of New Mexico, 210 Yale Blvd NE, Albuquerque, NM 87106, USA

Corresponding author: Romy Rodríguez

romy.rodriguez@cfa.harvard.edu

\* This paper includes data gathered with the 6.5 meter Magellan Telescopes located at Las Campanas Observatory, Chile.

## ABSTRACT

We present the detection and characterization of TOI-4994b (TIC 277128619b), a warm Saturn-sized planet discovered by the NASA Transiting Exoplanet Survey Satellite (TESS). TOI-4994b transits a G-type star ( $V = 12.6$  mag) with a mass, radius, and effective temperature of  $M_\star = 1.005^{+0.064}_{-0.061} M_\odot$ ,  $R_\star = 1.055^{+0.040}_{-0.037} R_\odot$ , and  $T_{\text{eff}} = 5640 \pm 110$  K. We obtained follow-up ground-based photometry from the Las Cumbres Observatory (LCO) and the Antarctic Search for Transiting ExoPlanets (ASTEP) telescopes, and we confirmed the planetary nature of TOI-4994b with multiple radial velocity observations from the PFS, CHIRON, HARPS, FEROS, and CORALIE instruments. From a global fit to the photometry and radial velocities, we determine that TOI-4994b is in a 21.5-day, eccentric orbit ( $e = 0.32 \pm 0.04$ ) and has a mass of  $M_P = 0.280^{+0.037}_{-0.034} M_J$ , a radius of  $R_P = 0.762^{+0.030}_{-0.027} R_J$ , and a Saturn-like bulk density of  $\rho_P = 0.78^{+0.16}_{-0.14}$  g/cm<sup>3</sup>. We find that TOI-4994 is a potentially viable candidate for follow-up stellar obliquity measurements. TOI-4994b joins the small sample of warm Saturn analogs and thus sheds light on our understanding of these rare and unique worlds.

*Keywords:* exoplanets - techniques: radial velocities - techniques: spectroscopic - techniques: photometric - methods: observational

## 1. INTRODUCTION

The number of known giant exoplanets has vastly expanded since the discovery of the first transiting giant planet (Charbonneau et al. 2000; Henry et al. 2000) with the advent of many wide-field transit and radial velocity (RV) surveys (e.g., Bakos et al. 2007, 2013; Pollacco et al. 2006; Pepper et al. 2007; Borucki et al. 2010). However, despite the thousands of giant planet discoveries brought about by these dedicated surveys, there are still many open questions regarding the formation mechanisms, composition, and evolution of these planets. One such longstanding problem in planetary astrophysics is whether close-in giant planets form in situ or instead form at larger orbital separations beyond the snowline and subsequently migrate inwards through interactions with the protoplanetary disk (e.g., Kley & Nelson 2012; Nelson 2018). In addition, the migration pathways of these planets are poorly understood (see, e.g., Winn & Fabrycky (2015), Dawson & Johnson (2018) and Schulte et al. 2024).

Transiting giant planets offer important clues to some of these problems, as they are comparatively easier to detect than small planets and are rich targets for characterization. First, they enable precise measurements of masses, radii, and orbital properties, providing valuable insights into their bulk composition and interior structure (Fortney et al. 2007; Fortney & Nettelmann 2010). The study of these objects refines and contextualizes our knowledge of the giant planets in our Solar System, while allowing us to explore the extreme physics of other types of planets that are not present within it. The relatively larger scale heights of giant planets (i.e., planet-to-star radius ratio) make them excellent targets for follow-up atmospheric characterization, pro-

viding clues about their heavy-element mass, interior structure and formation histories (Madhusudhan et al. 2014; Thorngren et al. 2016). These planets are also particularly well-suited for measurements of the sky-projected spin-orbit angle with the Rossiter-McLaughlin effect or Doppler Tomography (Gaudi & Winn 2007).

Warm giant planets, which have equilibrium temperatures below  $\sim 1000$  K, or orbital periods between 10–200 d ( $a \gtrsim 0.1$  AU), are uniquely interesting because, at their larger distances from their host stars, they are likely not subjected to the same physical processes that inflate the atmospheres of hot Jupiters (Fortney & Nettelmann 2010; Jordán et al. 2019; Müller & Helled 2023). Therefore, their observed properties are likely primordial and enable comparisons between planets at close distances from their host stars. However, the number of well-characterized warm transiting giants is still small, partly because the transit and RV methods are both biased towards planets on shorter periods. Additionally, most of the warm giants discovered from space missions like *Kepler* and CoRoT orbit fainter stars that are not especially amenable to follow-up observations. In fact, as of August 9, 2024, warm giants comprise only 17% (180 planets) of all known giants.<sup>1</sup>

The NASA Transiting Exoplanet Survey Satellite (TESS; Ricker et al. 2015) has been tremendously successful at finding all kinds of exoplanets, and it is expected to find over 250 giant planets with 2-minute cadence (Barclay et al. 2018). In this paper, we present the discovery of the warm Saturn TOI-4994b, which orbits a moderately bright ( $V = 12.6$  mag) G-type star on

<sup>1</sup> Data from the NASA Exoplanet Archive.

**Table 1.** Stellar Properties from the Literature.

Parameter	Value	Source
<b>Identifiers</b>		
TIC ID	277128619	1
TOI	4994	1
2MASS	J18523181-7826041	1
Gaia DR3	6364463103935391232	1
<b>Coordinates and Proper Motion</b>		
Right Ascension (RA)	18:52:31.81	2
Declination (Dec)	-78:26:03.95	2
$\mu_\alpha$ (mas yr <sup>-1</sup> )	0.897 ± 0.009	2
$\mu_\delta$ (mas yr <sup>-1</sup> )	9.90 ± 0.01	2
Gaia Parallax (mas)	3.022 <sup>+0.022</sup> <sub>-0.023</sub>	2
Distance (pc)	330.9 <sup>+2.5</sup> <sub>-2.4</sub>	3
<b>Broadband Magnitudes</b>		
Gaia <i>G</i> mag.	12.4792 ± 0.0001	2
Gaia <i>G<sub>BP</sub></i> mag.	12.913 ± 0.001	2
Gaia <i>G<sub>RP</sub></i> mag.	11.9044 ± 0.0007	2
TESS mag.	11.954 ± 0.006	4
2MASS <i>J</i> mag.	11.221 ± 0.021	5
2MASS <i>H</i> mag.	10.85 ± 0.02	5
2MASS <i>K<sub>S</sub></i> mag.	10.797 ± 0.022	5
<i>WISE 1</i> mag.	10.734 ± 0.023	6
<i>WISE 2</i> mag.	10.793 ± 0.021	6
<i>WISE 3</i> mag.	10.684 ± 0.068	6

**NOTES:** References: <sup>1</sup>SIMBAD Astronomical Database, <sup>2</sup>Gaia Collaboration et al. (2023), <sup>3</sup>This work, <sup>4</sup>TIC-v8.2 (Stassun et al. 2019), <sup>5</sup>Cutri et al. (2003), <sup>6</sup>Zacharias et al. (2017).

an eccentric, 21.5-day period orbit, discovered with data from TESS. The signals were followed up and confirmed as planetary with a suite of ground-based photometry from Las Cumbres Observatory (Brown et al. 2013) and the ASTEP-Antarctica observatory (Daban et al. 2010), and radial velocity observations from multiple spectrographs. The unique properties of Saturn analogs along with their relative rarity make them valuable laboratories to test and refine theories of planet formation. This paper is structured as follows. In Section 2, we provide confirmation of the planetary nature of TOI-4994b from our photometric and spectroscopic observations. In Section 3, we present our analysis of the data. In Section 4, we present our results and the properties of the planet in the context of the known exoplanet population; and we finally conclude in Section 5.

## 2. OBSERVATIONS

TOI-4994 (TIC 277128619) is a moderately bright ( $V=12.6$  mag) G-type star located at RA =

$18^h52^m31^s.81$  and Dec =  $-78^\circ26'03''95$ , at a distance of  $330.9 \pm 2.45$  pc (see Table 1 and Section 3 for more on the properties of the host). A transit-like signal with a period of 21.5 days was first detected in Sector 12 of TESS and subsequently confirmed with follow-up photometry from the ground. We describe these and the radial velocity observations in detail in the following subsections.

### 2.1. TESS Photometry

Since its launch in 2018, the TESS mission has found thousands of transiting exoplanet candidates around the nearest and brightest dwarf stars. TESS has four cameras that survey 95% of the sky. Currently, over 400 exoplanets have been confirmed or statistically validated, and we expect many more to follow.

TOI-4994b (TIC 277128619b) was first observed in Sectors 12 and 13 in June-July 2019 by Camera 3 at 30-minute cadence, and then again in Sectors 27 (July 2020) and 39 (June 2021) at 10-minute cadence, and finally in Sectors 66 and 67 in June-July 2023 at 2-minute cadence (Stumpe et al. 2012, 2014; Smith et al. 2012). A total of 11 TESS transits were observed across these sectors. The target will also be re-observed in 2025 in June and July. Data from all six sectors were used in our analysis.

The TESS data were processed and reduced with the NASA Science Processing Operations Center pipeline (SPOC; Jenkins et al. 2016; Caldwell et al. 2020), which searches for and identifies transit-like signals in the data. A threshold-crossing event was detected at 21.5 days using a Box Least Squares (BLS) algorithm, identifying the target as a TESS Object of Interest (TOI). The light curves were then downloaded using the `lightkurve` package (Lightkurve Collaboration et al. 2018), which retrieves data from the Barbara A. Mikulski Archive for Space Telescopes (MAST<sup>2</sup>). Finally, the light curves were flattened using `keplersplinev2`<sup>3</sup> (Vanderburg & Johnson 2014), which removes any out-of-transit variability due to stellar activity. The timeseries and phase-folded TESS transit light curves are shown in Figures 1 and 2.

### 2.2. Ground-based Photometry

The TESS pixel scale is  $\sim 21''$  pixel<sup>-1</sup> and photometric apertures typically extend out to roughly 1 arcminute, generally causing multiple stars to blend in the photometric aperture. To determine the true source of the TESS detection, we acquired ground-based time series follow-up photometry of the field around TOI-4994 as

<sup>2</sup> <https://mast.stsci.edu/portal/Mashup/Clients/Mast/Portal.html>

<sup>3</sup> <https://github.com/avanderburg/keplersplinev2>

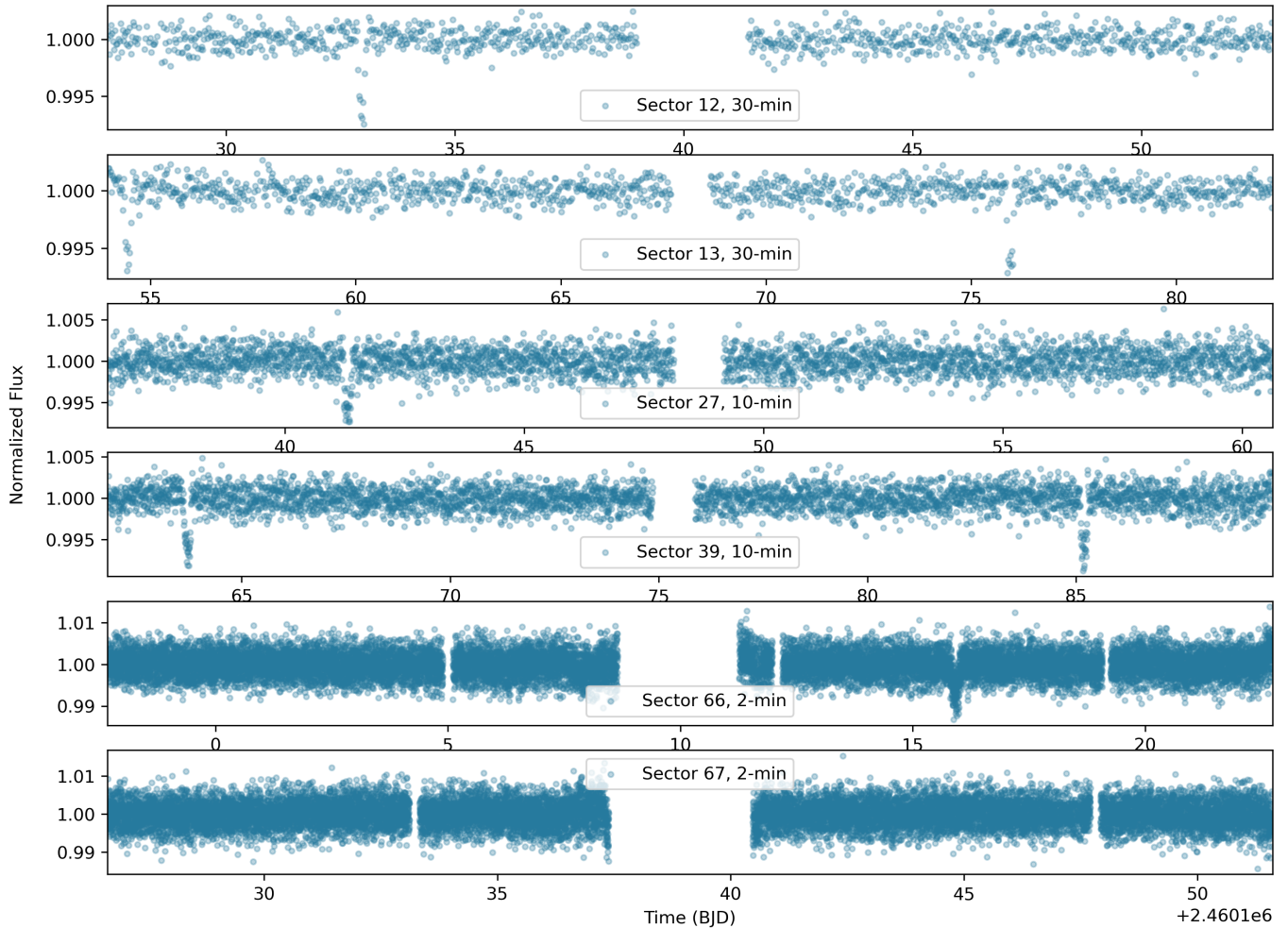


**Figure 1.** Time-series photometry of all 6 TESS sectors used in our analysis.

part of the TESS Follow-up Observing Program (TFOP; Collins 2019)<sup>4</sup>. We used the TESS Transit Finder, which is a customized version of the Tapir software package (Jensen 2013), to schedule our transit observations.

### 2.2.1. LCOGT

Follow-up light curve observations were taken with the Las Cumbres Observatory Global Telescope (LCOGT; Brown et al. 2013) 1-m network nodes at the South African Astronomical Observatory (SAAO) in Cape Town, South Africa and Cerro Tololo Interamerican Observatory (CTIO) in Chile. A full transit was observed simultaneously in  $g'$  and  $i'$  bands on July 11, 2023 from SAAO and an ingress observation was conducted simultaneously in  $g'$  and  $i'$  bands on May 8, 2023 from CTIO. The 1-m telescopes are equipped with  $4096 \times 4096$

SINISTRO cameras with an image scale of  $0''.389$  per pixel, resulting in a field of view of  $26' \times 26'$ . The images were calibrated by the standard LCOGT BANZAI pipeline (McCully et al. 2018), and differential photometric data were extracted using AstroImageJ (Collins et al. 2017). Circular photometric apertures with a  $4''.3$  radius were used, effectively excluding most of the flux from the nearest known neighbor in the *Gaia* DR3 catalog, which is  $6''$  west of TOI-4994 and is 6.6 magnitudes fainter in the TESS band. The light curve data are included in the global modeling described in Section 3 and the phase-folded transits are shown in Figure 3.

### 2.2.2. ASTEP-ANTARCTICA

We obtained follow-up photometric observations of TOI-4994 with the Antarctic Search for Transiting Exoplanets (ASTEP) telescope. ASTEP is a 0.4-m telescope located at Concordia station in Antarctica (Guillot et al. 2015; Mékarnia et al. 2016). It is equipped with two back-illuminated cameras operating in the  $B+V$

<sup>4</sup> <https://tess.mit.edu/followup>

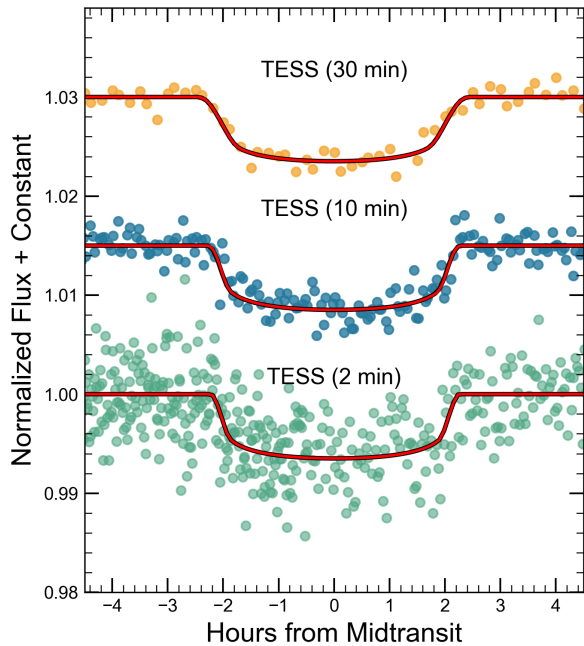


**Figure 2.** TESS light curves of TOI-4994 at 30 (top), 10 (middle), and 2 (bottom) minute cadences, combining 6 different sectors. The red lines show the best-fit EXOFASTv2 models, phase-folded on the orbital period.

bands, similar to *Gaia-B* (FLI Kepler KL400 sCMOS camera,  $2048 \times 2048$  pixels), and in a red band close to the *Gaia - R* band (Andor iKon-L 936 CCD camera,  $2048 \times 2048$  pixels). These cameras have an image scale of  $1.05''$  and  $1.30'' \text{ pixel}^{-1}$  respectively, resulting in corrected fields of view of  $36 \times 36 \text{ arcmin}^2$  and  $44 \times 44 \text{ arcmin}^2$  (Schmider et al. 2022). The data are processed on-site using IDL (Mékarnia et al. 2016) and Python aperture photometry pipelines (Dransfield et al. 2022).

Four observations of TOI-4994 were carried out with ASTEP, all under good weather conditions. A full transit of TOI-4994b was observed on UT 2022 August 23 in the *R*-band and on UT 2023 May 8 in the *B* and *R* bands, while two egress observations were observed on UT 2023 March 26 and on UT 2023 May 29, both in the *B* and *R* bands. The phase-folded transits are shown in Figure 3.

### 2.3. Spectroscopic Observations

We obtained follow-up radial velocity observations from multiple spectrographs to constrain the mass and orbit of TOI-4994b, which we describe in detail below. To assess whether the star is magnetically active, we cal-

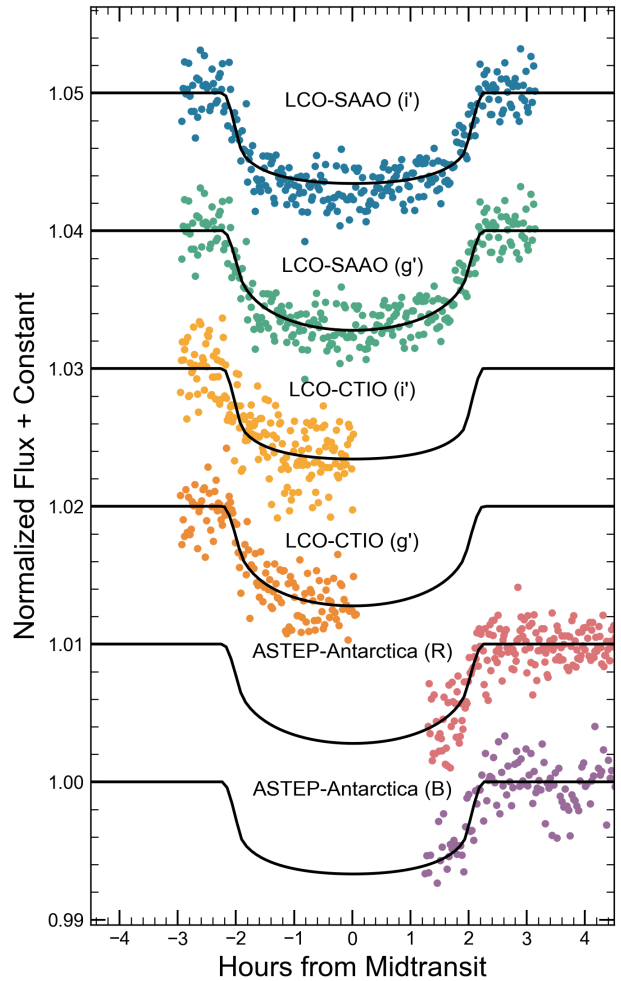


**Figure 3.** Light curves of TOI-4994 from the LCO and ASTEP-Antarctica ground-based observatories.

culated its chromospheric activity index,  $R'_{\text{HK}}$ , which is based on the flux emitted by Ca II H and K lines. The  $R'_{\text{HK}}$  index is the fraction of the star's bolometric luminosity emitted in these lines through magnetic activity. Using the empirical  $\text{NUV}-R'_{\text{HK}}$  relations from Findeisen et al. (2011), we obtained  $\log R'_{\text{HK}} = -5.06 \pm 0.05$ , which is near the minimum value of the chromospheric activity index for stars with solar metallicity of  $\log R'_{\text{HK}} = -5.08$ . We therefore treat TOI-4994 as an inactive star. All the RV datasets are shown as a function of time and phase-folded on the best-fit period in Figures 4 and 5 and listed in the Appendix (A).

#### 2.3.1. Planet Finder Spectrograph (PFS)

We collected 15 RV measurements of TOI-4994 between UT 2023 July 28 and UT 2023 September 25 with the Carnegie Planet Finder Spectrograph (PFS; Crane et al. 2006; Crane et al. 2008; Crane et al. 2010). PFS

is a high-precision echelle spectrograph attached to the 6.5-m Magellan Clay telescope at Las Campanas Observatory in Chile. It has a spectral resolution of 130,000 and covers the 390 – 734 nm spectral window. Wavelength calibration is carried out using an iodine absorption cell, which also allows for characterisation of the instrumental profile. Spectra were reduced using the standard PFS reduction pipeline (Butler et al. 1996; Crane et al. 2006) and radial velocity measurements were extracted using a custom IDL pipeline.

### 2.3.2. CHIRON

We obtained 15 spectra of TOI-4994 with the CHIRON high-resolution spectrograph on the SMARTS 1.5-m telescope located at CTIO in Chile. CHIRON is a fiber-fed echelle spectrograph with a resolving power of  $R = 80,000$  over the wavelength range 4100 – 8700 Å (Tokovinin et al. 2013). The observations were taken between UT 2022 August 28 and October 24. Wavelength calibrations are provided by bracketing Thorium-Argon (Th-Ar) arc lamp exposures. Relative velocities were measured from each spectrum by deriving their stellar line broadening kernels via a Least Squares Deconvolution (LSD) analysis (described in Zhou et al. 2016).

### 2.3.3. HARPS

We obtained a total of 10 RV measurements from the High Accuracy Radial velocity Planet Searcher (HARPS; Mayor et al. 2003) on the 3.6-m European Southern Observatory (ESO) telescope in La Silla Observatory, Chile. HARPS is a high-resolution spectrograph with a precision on the order of 1 m/s, a resolving power of 115,000 and a wavelength range of 378 – 691 nm. The spectra and radial velocities were reduced with the HARPS dedicated pipeline. The HARPS observations of our target were taken by two independent teams and therefore reduced with different methodologies. We label these HARPS-1 and HARPS-2 to distinguish them. In Figure 5, we plot only the most precise radial velocity data from PFS and HARPS to better highlight the best-fit RV model.

### 2.3.4. CORALIE

TOI-4994 was observed by the CORALIE fiber-fed high-resolution echelle spectrograph located at the Swiss 1.2-m Leonhard Euler Telescope at ESO’s La Silla Observatory (Udry et al. 2000; Queloz et al. 2001). It has a spectral resolution of 60,000 and a wavelength range of 390 – 680 nm. A total of 7 RV observations of TOI-4994 were collected between UT 2022 April 11 and September 23. The observations have exposure times of 1800 seconds and a signal-to-noise ratio (S/N) ranging between 25 and 50 measured at 550 nm. The S/N varia-

tions are due to the different observing conditions. The RVs were obtained by cross-correlating each spectrum against a binary mask corresponding to the stellar type G2 (e.g., Pepe et al. 2002). The resulting product is a cross-correlation function (CCF) from which the radial velocity is measured as well as several other indicators, such as the full width half maximum of the CCF, the bisector inverse slope and the contrast of the CCF. Additional indexes such as  $H_\alpha$  and Ca indexes are also derived from each spectrum.

### 2.3.5. FEROS

Additionally, we obtained a total of 20 RV observations with the ESO’s Fiber-fed Extended Range Optical Spectrograph (FEROS Kaufer et al. 1999) located at La Silla Observatory in Chile. These observations were obtained in the context of the Warm gIaNts with tEss (WINE) collaboration, which focuses on the systematic discovery and characterization of transiting warm giant planets (e.g. Brahm et al. 2019; Jordán et al. 2020; Brahm et al. 2020; Schlecker et al. 2020; Hobson et al. 2021; Trifonov et al. 2021, 2023; Brahm et al. 2023; Hobson et al. 2023; Eberhardt et al. 2023). FEROS has a spectral resolution of 48,000 and a wavelength coverage of 350 – 920 nm. Observations of TOI-4994 were taken between UT 2022 July 3 and UT 2023 September 7, with exposure times of 1200 seconds and S/Ns between 30 and 50 per resolution element. FEROS data was processed with the *ceres* pipeline (Brahm et al. 2017), which delivers precision radial velocities, bisector span measurements and a rough estimation of the atmospheric stellar parameters.

## 2.4. High-resolution Imaging with SOAR

We obtained high-resolution speckle images of TOI-4994 to check that the signals originate from the target star and not from another nearby stellar companion that could contaminate the SED and affect the inferred transit depth. The star was observed with the speckle camera at the Southern Astrophysical Research (SOAR) 4.1-m telescope on UT 2022 August 18. The data reduction process, as well as a thorough description of the SOAR-TESS survey can be found in Tokovinin (2018) and in Ziegler et al. (2019). In Figure 6, we show the  $5\sigma$  limit of companion detection, and the inset shows the speckle auto-correlation function (ACF). From this observation, we can exclude the presence of any stellar companion within about 4.5 magnitudes of the brightness of TOI-4994 and an angular separation between  $0.25''$  and  $2''$ , and within about 5 magnitudes for larger separations.

## 3. GLOBAL ANALYSIS

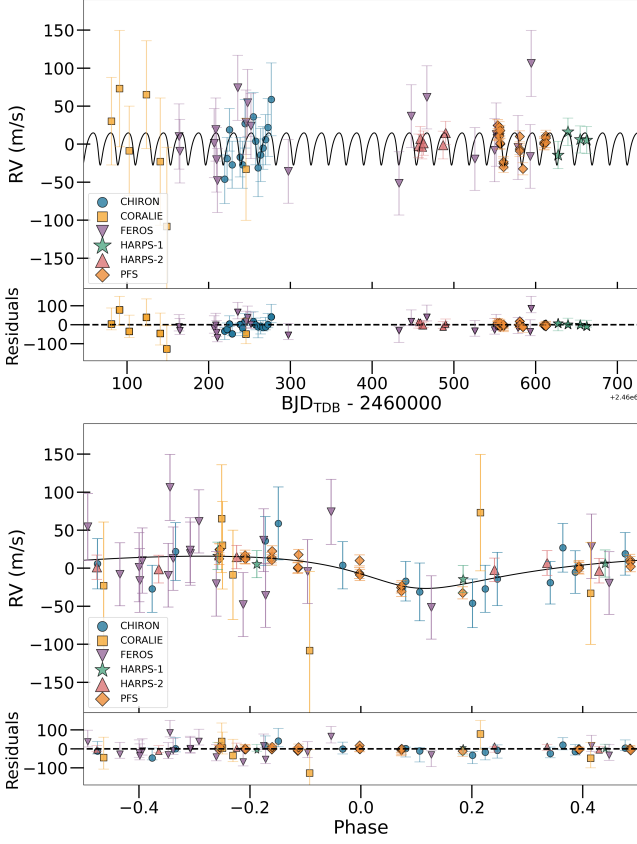


**Figure 4.** Radial velocity measurements of TOI-4994 (**top**) phase-folded on the orbital period (**bottom**). The black lines show the best-fit EXOFASTv2 models, with the residuals shown below the RV curves.

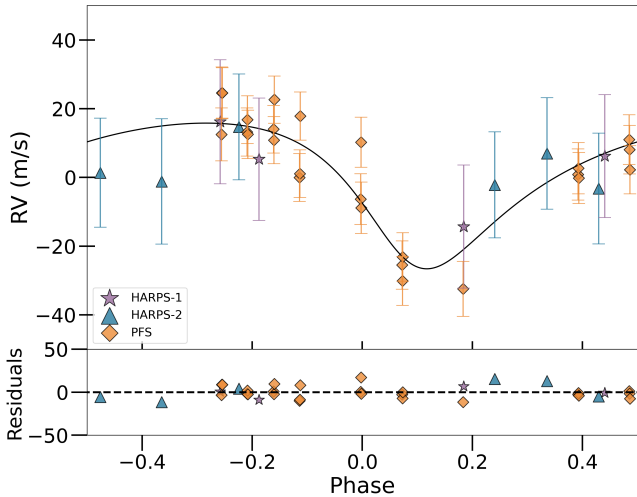


**Figure 5.** Phase-folded radial velocities from PFS (golden diamonds) and HARPS (purple stars and blue triangles) only, with residuals plotted below.

To constrain the stellar and planetary parameters of the system, we conducted a global fit of all our data

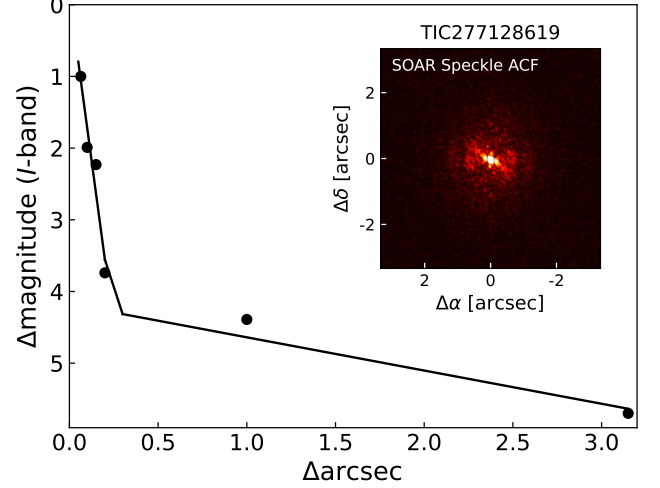


**Figure 6.** *I*-band speckle image and sensitivity curve for TOI-4994 from the Southern Astrophysical Research (SOAR) telescope.

using the publicly available exoplanet modeling suite, EXOFASTv2 (Eastman et al. 2013; Eastman 2017; Eastman et al. 2019). The physical properties of the host star were determined from a combination of the spectral energy distribution (SED) fit, as well as spectroscopic priors from our CHIRON data (including an initial estimate of the effective temperature and  $\log g$ ), a parallax prior from *Gaia* DR3 (Gaia Collaboration et al. 2023), and an upper bound on the extinction from galactic dust maps. For the SED fit, we incorporated available photometry from *Gaia* *G*, *G<sub>BP</sub>*, and *G<sub>RP</sub>* bands, 2MASS *J*, *H*, and *K* magnitudes, and WISE *W<sub>1</sub>* – *W<sub>4</sub>* magnitudes (see Table 1 for these values). A Kurucz (1992) atmosphere model was fit to all the available fluxes. As priors to the SED and global fit, we adopted a parallax of  $\mu = 3.022^{+0.022}_{-0.023}$  mas from *Gaia* EDR3 (corrected as per Lindegren et al. 2021) We set an upper limit on the maximum line-of-sight visual extinction  $A_V$  of 0.350 from the Schlegel et al. (1998) extinction maps. We used a prior on  $[\text{Fe}/\text{H}]$  of  $0.11 \pm 0.09$  dex, which is the median metallicity of all our spectra from CHIRON.

Within this SED fit, we use the MESA Isochrones and Stellar Tracks (MIST) stellar evolution models (Dotter 2016). Figure 7 illustrates the resulting SED fit, while the MIST evolutionary track is shown in Figure 8. The inferred stellar parameters are summarized in Table 2.

We infer a stellar mass of  $M_\star = 1.005^{+0.064}_{-0.061} M_\odot$ , a radius of  $R_\star = 1.055^{+0.040}_{-0.037} R_\odot$ , and an effective temperature of  $T_{\text{eff}} = 5640 \pm 100$  K, making this host a middle-aged ( $6.3^{+4.2}_{-3.8}$  Gyr) G5 dwarf (per the classifications by Pecaut & Mamajek 2013) and an almost identical solar twin. The star exhibits a slightly enhanced metallic-

ity, however, with  $[\text{Fe}/\text{H}] = 0.165^{+0.083}_{-0.084}$  dex. Using the empirical  $R'_{\text{HK}}$ -age relations by Mamajek & Hillenbrand (2008), we derived an age for the system of  $7.8 \pm 1.3$  Gyr, which is consistent with the age from our SED fit. These relations also predict a stellar rotation period of  $46.2 \pm 3.1$  days.

The planetary parameters were determined through a simultaneous global fit of the system, which combined the TESS and ground-based photometry and the six RV datasets described in Sections 2.1, 2.2, and 2.3. EXOFASTv2 determines the stellar and planetary parameters using a differential evolution Markov Chain Monte Carlo method (see Eastman et al. 2013 for further details). We adopted an initial guess on the ephemeris from an independent fit to the TESS light curves. The resulting planetary parameters are listed in Table 3.

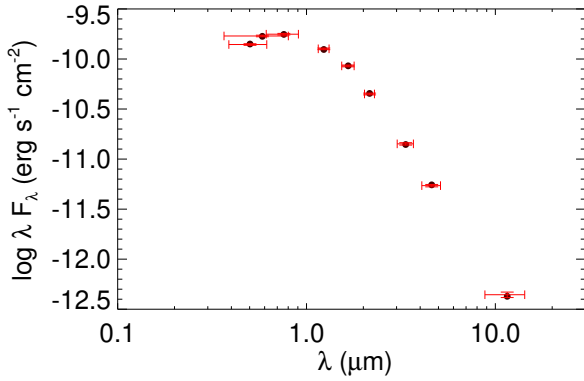


**Figure 7.** Spectral Energy Distribution (SED) fit for TOI-4994. The horizontal error bars correspond to the bandwidth of each filter, while the error bars in flux are the measurement uncertainties. The black points are the modeled, broadband averages.

#### 4. RESULTS AND DISCUSSION

From our global fit to the available photometry and radial velocity datasets, we determined a planetary mass of  $M_P = 0.280^{+0.037}_{-0.034} M_J$  (or  $89.1 M_{\oplus}$ ), a radius of  $R_P = 0.762^{+0.030}_{-0.027} R_J$  (or  $8.55 R_{\oplus}$ ), and a bulk density of  $\rho_p = 0.78^{+0.16}_{-0.14} \text{ g/cm}^3$ . These properties are similar to those of Saturn, and, given the planet’s orbital period, it fits in with the population of warm Saturns. The number of well-characterized warm Saturns in the literature is still small. There are currently less than 20 planets between  $0.8\text{--}1.1 M_{\text{Sat}}$  and with periods between 10–200 days that have directly measured masses and radii, making this object a valuable addition to this rare sample. Some of these include HD 89345b (Van Eylen et al. 2018), K2-287b (Jordán et al. 2019), K2-261b (Johnson et al. 2018),

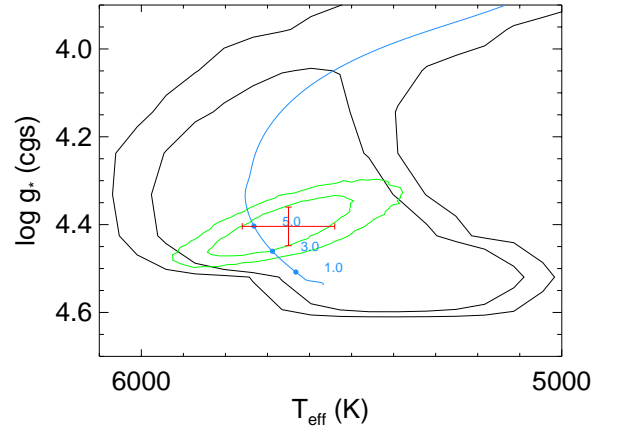


**Figure 8.** Evolutionary track and present evolutionary stage of TOI-4994 based on the best-fit MIST model. The blue line is the MIST track and the black contours represent the  $1\sigma$  and  $2\sigma$  constraints on the current temperature and surface gravity from the MIST isochrone, while the green contours show the  $1\sigma$  and  $2\sigma$  constraints on  $T_{\text{eff}}$  and  $\log g_*$  from the EXOFASTv2 fit and observations of the system. The red cross indicates the median value and confidence intervals.

NGTS-11b (TOI-1847b; Gill et al. 2020), and K2-232b (Brahm et al. 2020).

Although the mass and radius of TOI-4994b are slightly too large to categorize it as a sub-Saturn, (typically defined as planets with  $4 < R_p/R_{\oplus} < 8$ ) it shares many characteristics with this population, described in detail by Petigura et al. (2017). Notably, TOI-4994b is a single planet (with no evidence of other companions in the system), and has an eccentric orbit ( $e = 0.32^{+0.048}_{-0.047}$ ). Such high eccentricity and lack of observed companions (characteristic of the most massive sub-Saturns) may be evidence of past dynamical instability, as hypothesized by Petigura et al. (2017). In addition, TOI-4994b orbits a metal-rich star ( $[\text{Fe}/\text{H}] = 0.165^{+0.083}_{-0.084}$  dex), like the majority of known sub-Saturns. Interestingly, Petigura et al. (2017) also found strong correlations between planet mass, eccentricity, and host star metallicity.

Fairnington et al. (in prep) identified a potential bimodality in the eccentricity distribution of warm, single sub-Saturns, noting a scarcity of moderately eccentric planets ( $e = 0.2 - 0.5$ ). TOI-4994b is the third confirmed object in this range, and its properties suggest a history shaped by planet-planet scattering and a possible merger (Petigura et al. 2017; Brady et al. 2018; Millholland et al. 2022). If a merger were the origin history of this planet, it may have a high bulk metallicity, which could be probed with JWST. While TOI-4994b’s eccen-

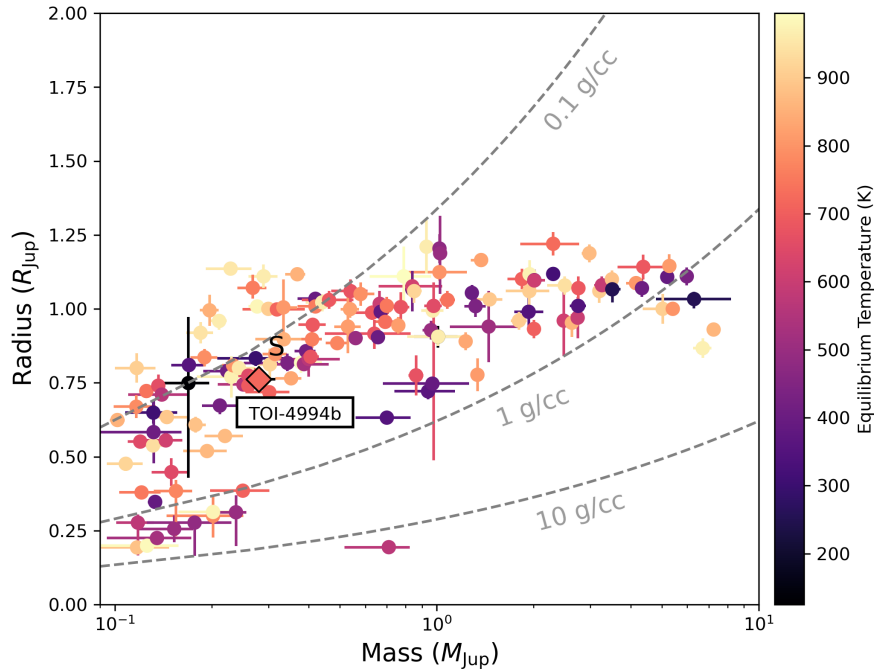


**Figure 9.** Mass-radius diagram of all warm giants (planet masses between  $0.1 \leq M_{\text{Jup}} \leq 10$  and temperatures below 1000 K). The grey dashed lines are lines of constant bulk density. TOI-4994b is represented by a diamond, and Saturn is over-plotted for reference.

tricity and orbital distance are inconsistent with high eccentricity migration, additional radial velocity follow-up to search for long-period non-transiting companions may provide additional insights into its formation history.

TOI-4994b has a relatively high equilibrium temperature of  $717.6^{+9.7}_{-10}$  K, calculated using Equation 1 from Hansen & Barman (2007) within EXOFASTv2:

$$T_{eq} = T_{\text{eff}} \sqrt{\frac{R_{\star}}{2a}}, \quad (1)$$

and which assumes an albedo of zero and perfect heat redistribution. We also estimate an orbit-averaged incident flux of  $5.4 \times 10^7 \text{ erg s}^{-1} \text{ cm}^{-2}$ , using the following formula:

$$\langle F \rangle = \sigma_B T_{\text{eff}}^4 \left( \frac{R_{\star}}{a} \left( 1 - e^2/2 \right) \right)^2, \quad (2)$$

and we find that TOI-4994b is below the Demory & Seager (2011) insolation threshold of  $2 \times 10^8 \text{ erg s}^{-1} \text{ cm}^{-2}$ . Figure 9 highlights the mass and radius of TOI-4994b within the population of warm giant planets in the NASA Exoplanet Archive (Akeson et al. 2013). The planets are color-coded by their reported equilibrium temperature.

The atmospheric composition of a planet provides key insights into its formation, history, and potential for habitability (see, e.g., Madhusudhan 2019). In order to assess the prospects for follow-up atmospheric characterization of TOI-4994b with JWST, we evaluated its Transmission Spectroscopy Metric (TSM; Kempton et al. 2018). This value is proportional to the expected signal-to-noise ratio of a transmission spectrum of the target, with higher numbers indicating better prospects for observation. We obtained a TSM value of 30 for TOI-4994b, which is below the value of 90 recommended by Kempton et al. (2018) for planets between  $4\text{--}10R_{\oplus}$ .

Finally, we consider the feasibility of measuring the spin-orbit misalignment of the system via the Rossiter-McLaughlin (RM) effect or Doppler Tomography. We estimate an expected RM signal of 8.3 m/s for TOI-4994b using Equation 12 of Albrecht et al. (2022), assuming a rotational velocity of  $v \sin i_{\star} = 2.2 \text{ km/s}$ , which is a typical value for G-type stars (e.g., dos Santos et al. 2016). Alternatively, using the predicted stellar rotation rate of  $46.2 \pm 3.1$  days estimated in Section 3, we derived an RM signal of 4.3 m/s. Although TOI-4994 is slightly fainter than other stars hosting a warm giant, this signal is potentially observable with high-resolution instruments, such as PFS, and we therefore encourage

**Table 2.** Median values and 68% confidence interval for global model of TOI-4994

Parameter	Units	Values
$M_*$ . . . . .	Mass ( $M_\odot$ ) . . . . .	$1.005^{+0.064}_{-0.061}$
$R_*$ . . . . .	Radius ( $R_\odot$ ) . . . . .	$1.055^{+0.040}_{-0.037}$
$L_*$ . . . . .	Luminosity ( $L_\odot$ ) . . . . .	$1.020^{+0.041}_{-0.052}$
$F_{Bol}$ . . . . .	Bolometric Flux (cgs) . . . . .	$(2.98^{+0.11}_{-0.15}) \times 10^{-10}$
$\rho_*$ . . . . .	Density (cgs) . . . . .	$1.21^{+0.17}_{-0.16}$
$\log g$ . . . . .	Surface gravity (cgs) . . . . .	$4.393^{+0.045}_{-0.046}$
$T_{eff}$ . . . . .	Effective Temperature (K) . . . . .	$5640 \pm 110$
[Fe/H] . . . . .	Metallicity (dex) . . . . .	$0.165^{+0.083}_{-0.084}$
[Fe/H] <sub>0</sub> . . . . .	Initial Metallicity <sup>1</sup> . . . . .	$0.176^{+0.079}_{-0.080}$
$Age$ . . . . .	Age (Gyr) . . . . .	$6.3^{+4.2}_{-3.8}$
$EEP$ . . . . .	Equal Evolutionary Phase <sup>2</sup> . . . . .	$380^{+31}_{-41}$
$A_V$ . . . . .	V-band extinction (mag) . . . . .	$0.295^{+0.041}_{-0.073}$
$\sigma_{SED}$ . . . . .	SED photometry error scaling	$0.73^{+0.31}_{-0.19}$
$\varpi$ . . . . .	Parallax (mas) . . . . .	$3.022^{+0.022}_{-0.023}$
$d$ . . . . .	Distance (pc) . . . . .	$330.9^{+2.5}_{-2.4}$

**NOTES:**

See Table 3 in Eastman et al. (2019) for a detailed description of all parameters.

<sup>1</sup>The metallicity of the star at birth.

<sup>2</sup>Corresponds to static points in a star’s evolutionary history. See §2 in Dotter (2016).

future follow-up observations to determine the system’s spin-orbit alignment.

## 5. CONCLUSIONS

We presented the discovery and characterization of TOI-4994b, a warm Saturn transiting a moderately bright ( $V = 12.6$  mag) G-type star in an eccentric, 21.5-day orbit, discovered by TESS. We confirmed the planetary nature of TOI-4994 with extensive ground-based photometry and with multiple high-resolution radial velocities from CHIRON, PFS, HARPS, FEROS, and CORALIE, and we ruled out the presence of nearby stellar companions with SOAR images. From our observations, we determined that TOI-4994 has physical properties similar to Saturn’s, and consistent with the population of known sub-Saturns. We encourage further observations of this system, as it is a promising candidate for spin-orbit angle measurements via the Rossiter-MacLaughlin effect. Such observations could shed more light on the formation and evolution of these rare planets.

## ACKNOWLEDGEMENTS

RRM thanks Samuel Yee for conversations that improved this manuscript. T.T. acknowledges support by the BNSF program ”VIHREN-2021” project No. KP-06-DV/5. This paper includes data collected by the TESS mission. Funding for the TESS mission is provided by the NASA’s Science Mission Directorate. This research has also made use of the Exoplanet Follow-up Observation Program website, which is operated by

the California Institute of Technology, under contract with the National Aeronautics and Space Administration under the Exoplanet Exploration Program. This paper includes data gathered with the 6.5-meter Magellan Telescopes located at Las Campanas Observatory, Chile. Additionally, some observations were collected at the European Southern Observatory under ESO programmes 111.250B.001 and 112.25W1.001. ML acknowledges support of the Swiss National Science Foundation under grant number PCEFP2\_194576.

This work makes use of observations from the LCOGT network. Part of the LCOGT telescope time was granted by NOIRLab through the Mid-Scale Innovations Program (MSIP). MSIP is funded by NSF. Funding for the TESS mission is provided by NASA’s Science Mission Directorate. This work has made use of data from the European Space Agency (ESA) mission *Gaia* (<https://www.cosmos.esa.int/gaia>), processed by the *Gaia* Data Processing and Analysis Consortium (DPAC, <https://www.cosmos.esa.int/web/gaia/dpac/consortium>). The contributions of ML, SUM, MB, AP, PF, FB, and SU were carried out within the framework of the NCCR PlanetS supported by the Swiss National Science Foundation under grants 51NF40\_182901 and 51NF40\_205606. The postdoctoral fellowship of KB is funded by F.R.S.-FNRS grant T.0109.20 and by the Francqui Foundation. The results reported herein benefitted from collaborations and/or information exchange within NASA’s Nexus for Exoplanet System Science (NExSS) research coordination network sponsored by NASA’s Science Mission Directorate under Agreement

**Table 3.** Median values and 68% confidence interval for global model of TOI-4994 b

Parameter	Description (Units)	Values
$P$ .....	Period (days) .....	$21.491984 \pm 0.000023$
$R_P$ .....	Radius ( $R_J$ ) .....	$0.762^{+0.030}_{-0.027}$
$M_P$ .....	Mass ( $M_J$ ) .....	$0.280^{+0.037}_{-0.034}$
$T_C$ .....	Time of conjunction <sup>4</sup> (BJD <sub>TDB</sub> ) .....	$2459363.69480 \pm 0.00076$
$T_T$ .....	Time of minimum projected separation <sup>5</sup> (BJD <sub>TDB</sub> ) .....	$2459363.69484 \pm 0.00076$
$T_0$ .....	Optimal conjunction Time <sup>6</sup> (BJD <sub>TDB</sub> ) .....	$2459965.47035^{+0.00042}_{-0.00041}$
$a$ .....	Semi-major axis (AU) .....	$0.1515^{+0.0032}_{-0.0031}$
$i$ .....	Inclination (Degrees) .....	$89.56^{+0.29}_{-0.32}$
$e$ .....	Eccentricity .....	$0.319^{+0.048}_{-0.047}$
$\omega_*$ .....	Argument of Periastron (Degrees) .....	$143.1^{+9.5}_{-10.}$
$T_{eq}$ .....	Equilibrium temperature <sup>7</sup> (K) .....	$717.6^{+9.7}_{-10.}$
$\tau_{\text{circ}}^\dagger$ .....	Tidal circularization timescale (Gyr) .....	$610^{+400}_{-260}$
$K$ .....	RV semi-amplitude (m/s) .....	$21.6^{+2.3}_{-2.4}$
$R_P/R_*$ .....	Radius of planet in stellar radii .....	$0.07424^{+0.00078}_{-0.00068}$
$a/R_*$ .....	Semi-major axis in stellar radii .....	$30.9 \pm 1.4$
$\delta$ .....	$(R_P/R_*)^2$ .....	$0.00551^{+0.00012}_{-0.00010}$
$\delta_B$ .....	Transit depth in B (fraction) .....	$0.00829^{+0.00039}_{-0.00035}$
$\delta_R$ .....	Transit depth in R (fraction) .....	$0.00684^{+0.00025}_{-0.00024}$
$\delta_{g'}$ .....	Transit depth in g' (fraction) .....	$0.00788^{+0.00026}_{-0.00024}$
$\delta_{i'}$ .....	Transit depth in i' (fraction) .....	$0.00662 \pm 0.00016$
$\delta_{\text{TESS}}$ .....	Transit depth in TESS (fraction) .....	$0.00657 \pm 0.00013$
$\delta_V$ .....	Transit depth in V (fraction) .....	$0.00708^{+0.00025}_{-0.00024}$
$\tau$ .....	Ingress/egress transit duration (days) .....	$0.01319^{+0.0011}_{-0.00041}$
$T_{14}$ .....	Total transit duration (days) .....	$0.1855^{+0.0013}_{-0.0011}$
$T_{\text{FWHM}}$ .....	FWHM transit duration (days) .....	$0.17213^{+0.00092}_{-0.00091}$
$b$ .....	Transit Impact parameter .....	$0.18^{+0.14}_{-0.12}$
$b_S$ .....	Eclipse impact parameter .....	$0.26^{+0.18}_{-0.17}$
$\tau_S$ .....	Ingress/egress eclipse duration (days) .....	$0.0202^{+0.0024}_{-0.0019}$
$T_{S,14}$ .....	Total eclipse duration (days) .....	$0.265^{+0.029}_{-0.025}$
$T_{S,\text{FWHM}}$ .....	FWHM eclipse duration (days) .....	$0.245^{+0.028}_{-0.025}$
$\delta_{S,2.5\mu\text{m}}^\dagger$ .....	Blackbody eclipse depth at $2.5\mu\text{m}$ (ppm) .....	$3.22^{+0.39}_{-0.35}$
$\delta_{S,5.0\mu\text{m}}^\dagger$ .....	Blackbody eclipse depth at $5.0\mu\text{m}$ (ppm) .....	$67.8^{+4.5}_{-4.1}$
$\delta_{S,7.5\mu\text{m}}^\dagger$ .....	Blackbody eclipse depth at $7.5\mu\text{m}$ (ppm) .....	$165.5^{+8.4}_{-7.7}$
$\rho_P$ .....	Density (cgs) .....	$0.78^{+0.16}_{-0.14}$
$\log g_P$ .....	Surface gravity .....	$3.077^{+0.069}_{-0.074}$
$\langle F \rangle$ .....	Incident Flux ( $10^9 \text{ erg s}^{-1} \text{ cm}^{-2}$ ) .....	$0.0544^{+0.0029}_{-0.0031}$
$T_P$ .....	Time of Periastron (BJD <sub>TDB</sub> ) .....	$2459343.85^{+0.38}_{-0.35}$
$T_S$ .....	Time of eclipse (BJD <sub>TDB</sub> ) .....	$2459370.99^{+0.72}_{-0.74}$
$V_c/V_e$ .....	.....	$0.797 \pm 0.039$
$e \cos \omega_*$ .....	.....	$-0.250^{+0.053}_{-0.056}$
$e \sin \omega_*$ .....	.....	$0.189^{+0.048}_{-0.047}$

**NOTES:**

See Table 3 in [Eastman et al. \(2019\)](#) for a detailed description of all parameters.

<sup>†</sup> These values are predicted values from theory and not directly observed.

<sup>4</sup>Time of conjunction is commonly reported as the “transit time”.

<sup>5</sup>Time of minimum projected separation is a more correct “transit time”.

<sup>6</sup>Optimal time of conjunction minimizes the covariance between  $T_C$  and Period.

<sup>7</sup>Assumes no albedo and perfect redistribution.

No. 80NSSC21K0593 for the program “Alien Earths”. We acknowledge the use of public TESS data from pipelines at the TESS Science Office and at the TESS Science Processing Operations Center. Resources supporting this work were provided by the NASA High-End Computing (HEC) Program through the NASA Advanced Supercomputing (NAS) Division at Ames Research Center for the production of the SPOC data products.

Funding for the DPAC has been provided by national institutions, in particular the institutions participating in the *Gaia* Multilateral Agreement. Finally, this research has made use of the NASA Exoplanet Archive, which is operated by the California Institute of Technol-

ogy, under contract with the National Aeronautics and Space Administration under the Exoplanet Exploration Program. KAC acknowledges support from the TESS mission via subaward s3449 from MIT.

*Facilities:* TESS, LCOGT, ASTEP-Antarctica, PFS, HARPS, CHIRON, CORALIE, FEROS, SOAR, Exoplanet Archive.

*Software:* AstroImageJ (Collins et al. 2017), EXOFASTv2 (Eastman et al. 2019), numpy (Harris et al. 2020), TAPIR (Jensen 2013).

## APPENDIX

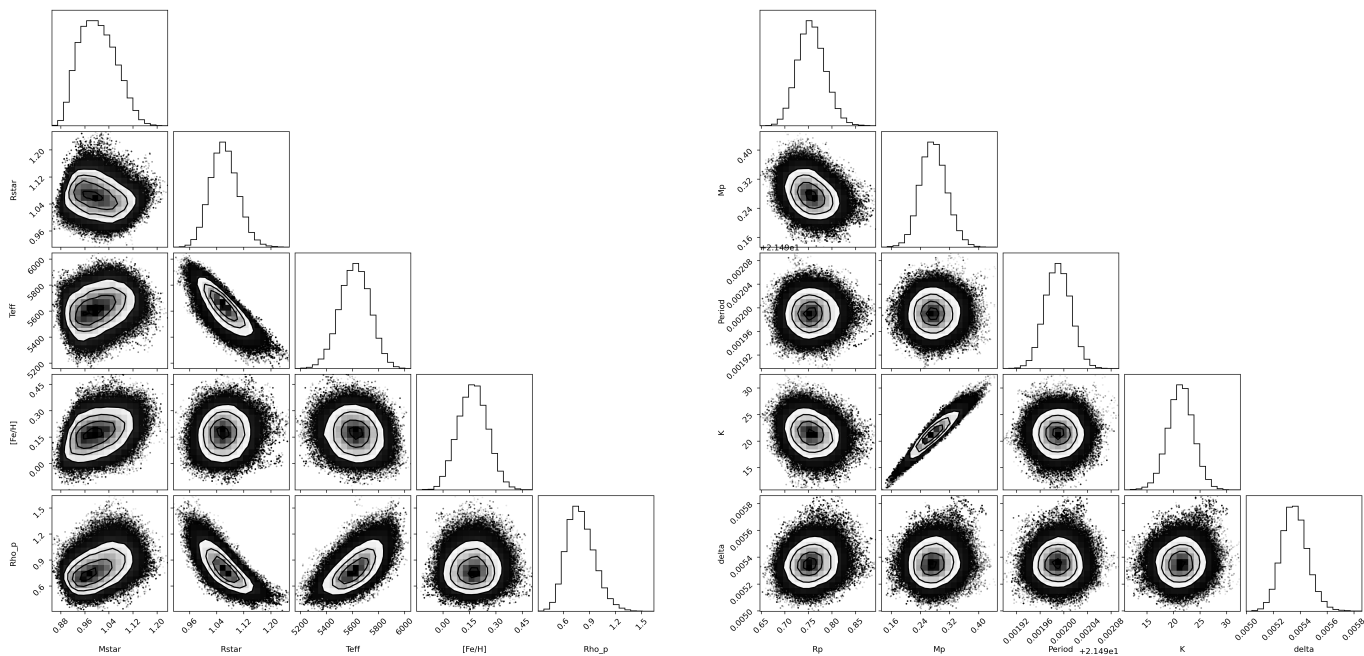


**Figure 10.** Corner plots showing the covariances for some of the stellar and planetary parameters in our analysis.

## A. RADIAL VELOCITY OBSERVATIONS

## REFERENCES

Akeson, R. L., Chen, X., Ciardi, D., et al. 2013, *PASP*, 125, 989, doi: [10.1088/672273](https://doi.org/10.1088/672273)

Albrecht, S. H., Dawson, R. I., & Winn, J. N. 2022, *PASP*, 134, 082001, doi: [10.1088/1538-3873/ac6c09](https://doi.org/10.1088/1538-3873/ac6c09)

**Table 4.** Radial Velocity Data

Time (BJD)	RV (m/s)	RV error (m/s)	Instrument
2460153.61049	4.40	4.13	Planet Finder Spectrograph
2460153.62499	16.50	3.84	Planet Finder Spectrograph
2460153.63926	16.49	3.43	Planet Finder Spectrograph
2460154.60562	5.10	2.63	Planet Finder Spectrograph
2460154.61980	8.69	2.45	Planet Finder Spectrograph
2460154.63393	4.43	2.66	Planet Finder Spectrograph
2460155.64044	5.92	2.36	Planet Finder Spectrograph
2460155.65419	2.74	2.21	Planet Finder Spectrograph
2460155.66844	14.53	2.18	Planet Finder Spectrograph
2460156.65824	-8.11	2.47	Planet Finder Spectrograph
2460156.67302	-7.01	2.44	Planet Finder Spectrograph
2460156.68696	9.74	2.66	Planet Finder Spectrograph
2460160.66059	-33.60	2.68	Planet Finder Spectrograph
2460160.67464	-38.21	2.89	Planet Finder Spectrograph
2460160.68876	-31.25	2.81	Planet Finder Spectrograph
2460180.53256	-14.42	3.48	Planet Finder Spectrograph
2460180.54735	2.14	3.30	Planet Finder Spectrograph
2460180.56107	-16.94	3.67	Planet Finder Spectrograph
2460184.54002	-40.53	4.71	Planet Finder Spectrograph
2460210.52069	-7.26	3.66	Planet Finder Spectrograph
2460210.53530	-5.42	3.68	Planet Finder Spectrograph
2460210.54950	-8.28	3.58	Planet Finder Spectrograph
2460212.51455	2.93	3.17	Planet Finder Spectrograph
2460212.52869	0.00	2.76	Planet Finder Spectrograph
2460212.54273	-5.89	2.62	Planet Finder Spectrograph
2459819.56147	5965.0	32.0	CHIRON
2459822.57141	5992.0	28.0	CHIRON
2459825.47184	6030.0	28.0	CHIRON
2459828.63916	5984.0	31.0	CHIRON
2459838.46341	5994.0	26.0	CHIRON
2459841.54330	5984.0	31.0	CHIRON
2459844.54869	6038.0	32.0	CHIRON
2459854.51278	6047.0	32.0	CHIRON
2459857.51441	6015.0	31.0	CHIRON
2459860.49822	5980.0	38.0	CHIRON
2459863.50449	5997.0	35.0	CHIRON
2459866.52502	6006.0	28.0	CHIRON
2459869.50415	6017.0	33.0	CHIRON
2459872.52953	6033.0	38.0	CHIRON
2459876.50716	6070.0	48.0	CHIRON
2459680.91764	5393.1	35.7	CORALIE
2459690.91570	5436.0	61.8	CORALIE
2459702.81753	5354.2	37.8	CORALIE
2459723.87356	5428.1	54.7	CORALIE
2459740.79469	5340.0	70.5	CORALIE
2459748.77041	5254.7	93.9	CORALIE
2459845.62784	5329.9	49.8	CORALIE

**Table 4.** Radial Velocity Datasets (Continued)

Time (BJD)	RV (m/s)	RV error (m/s)	Instrument
2459763.78280	5349.6	14.6	FEROS
2459764.78507	5330.3	11.4	FEROS
2459806.64321	5340.8	20.8	FEROS
2459808.62570	5358.8	10.1	FEROS
2459809.63296	5319.1	13.4	FEROS
2459810.67493	5291.7	12.0	FEROS
2459835.57461	5413.7	14.6	FEROS
2459847.63789	5393.9	17.4	FEROS
2459845.65994	5368.4	12.9	FEROS
2459851.60212	5363.3	14.1	FEROS
2459897.50622	5303.8	11.9	FEROS
2460032.88150	5288.0	10.3	FEROS
2460047.87740	5376.4	9.3	FEROS
2460066.86333	5401.1	9.8	FEROS
2460125.74290	5320.0	8.7	FEROS
2460149.76750	5331.6	9.9	FEROS
2460151.83118	5352.2	10.7	FEROS
2460178.52971	5335.2	12.1	FEROS
2460193.51918	5323.4	11.4	FEROS
2460194.69004	5445.8	16.0	FEROS
2460227.54377	5371.7	4.3	HARPS-1
2460239.52640	5402.2	4.8	HARPS-1
2460254.54061	5392.2	4.1	HARPS-1
2460262.53137	5391.3	3.7	HARPS-1
2460056.82106	5233.7	6.4	HARPS-2
2460058.85810	5242.8	8.2	HARPS-2
2460060.87608	5232.6	7.9	HARPS-2
2460062.90944	5237.2	7.4	HARPS-2
2460086.79806	5234.7	11.6	HARPS-2
2460089.81426	5250.6	6.3	HARPS-2

- Bakos, G. Á., Kovács, G., Torres, G., et al. 2007, *ApJ*, 670, 826, doi: [10.1086/521866](https://doi.org/10.1086/521866)
- Bakos, G. Á., Csabry, Z., Penev, K., et al. 2013, *PASP*, 125, 154, doi: [10.1086/669529](https://doi.org/10.1086/669529)
- Barclay, T., Pepper, J., & Quintana, E. V. 2018, *ApJS*, 239, 2, doi: [10.3847/1538-4365/aae3e9](https://doi.org/10.3847/1538-4365/aae3e9)
- Borucki, W. J., Koch, D., Basri, G., et al. 2010, *Science*, 327, 977, doi: [10.1126/science.1185402](https://doi.org/10.1126/science.1185402)
- Brady, M. T., Petigura, E. A., Knutson, H. A., et al. 2018, *AJ*, 156, 147, doi: [10.3847/1538-3881/aad773](https://doi.org/10.3847/1538-3881/aad773)
- Brahm, R., Jordán, A., & Espinoza, N. 2017, *PASP*, 129, 034002, doi: [10.1088/1538-3873/aa5455](https://doi.org/10.1088/1538-3873/aa5455)
- Brahm, R., Espinoza, N., Jordán, A., et al. 2019, *AJ*, 158, 45, doi: [10.3847/1538-3881/ab279a](https://doi.org/10.3847/1538-3881/ab279a)
- Brahm, R., Nielsen, L. D., Wittenmyer, R. A., et al. 2020, *AJ*, 160, 235, doi: [10.3847/1538-3881/abba3b](https://doi.org/10.3847/1538-3881/abba3b)
- Brahm, R., Ulmer-Moll, S., Hobson, M. J., et al. 2023, *AJ*, 165, 227, doi: [10.3847/1538-3881/accadd](https://doi.org/10.3847/1538-3881/accadd)
- Brown, T. M., Baliber, N., Bianco, F. B., et al. 2013, *PASP*, 125, 1031, doi: [10.1086/673168](https://doi.org/10.1086/673168)
- Butler, R. P., Marcy, G. W., Williams, E., et al. 1996, *Publications of the Astronomical Society of the Pacific*, 108, 500, doi: [10.1086/133755](https://doi.org/10.1086/133755)
- Caldwell, D. A., Tenenbaum, P., Twicken, J. D., et al. 2020, *Research Notes of the American Astronomical Society*, 4, 201, doi: [10.3847/2515-5172/abc9b3](https://doi.org/10.3847/2515-5172/abc9b3)
- Charbonneau, D., Brown, T. M., Latham, D. W., & Mayor, M. 2000, *ApJL*, 529, L45, doi: [10.1086/312457](https://doi.org/10.1086/312457)
- Collins, K. 2019, in *American Astronomical Society Meeting Abstracts*, Vol. 233, American Astronomical Society Meeting Abstracts #233, 140.05
- Collins, K. A., Kielkopf, J. F., Stassun, K. G., & Hessman, F. V. 2017, *AJ*, 153, 77, doi: [10.3847/1538-3881/153/2/77](https://doi.org/10.3847/1538-3881/153/2/77)
- Crane, J. D., Shectman, S. A., & Butler, R. P. 2006, in *Society of Photo-Optical Instrumentation Engineers (SPIE) Conference Series*, Vol. 6269, Society of Photo-Optical Instrumentation Engineers (SPIE) Conference Series, ed. I. S. McLean & M. Iye, 626931, doi: [10.1117/12.672339](https://doi.org/10.1117/12.672339)
- Crane, J. D., Shectman, S. A., Butler, R. P., et al. 2010, *Society of Photo-Optical Instrumentation Engineers (SPIE) Conference Series*, Vol. 7735, The Carnegie Planet Finder Spectrograph: integration and commissioning, 773553, doi: [10.1117/12.857792](https://doi.org/10.1117/12.857792)
- Crane, J. D., Shectman, S. A., Butler, R. P., Thompson, I. B., & Burley, G. S. 2008, in *Proceedings of the SPIE*, ed. I. S. McLean & M. M. Casali, 701479, doi: [10.1117/12.789637](https://doi.org/10.1117/12.789637)
- Cutri, R. M., Skrutskie, M. F., van Dyk, S., et al. 2003, *VizieR Online Data Catalog*, 2246, 0
- Daban, J.-B., Gouvret, C., Guillot, T., et al. 2010, in *Society of Photo-Optical Instrumentation Engineers (SPIE) Conference Series*, Vol. 7733, Ground-based and Airborne Telescopes III, ed. L. M. Stepp, R. Gilmozzi, & H. J. Hall, 77334T, doi: [10.1117/12.854946](https://doi.org/10.1117/12.854946)
- Dawson, R. I., & Johnson, J. A. 2018, *ARA&A*, 56, 175, doi: [10.1146/annurev-astro-081817-051853](https://doi.org/10.1146/annurev-astro-081817-051853)
- Demory, B.-O., & Seager, S. 2011, *ApJS*, 197, 12, doi: [10.1088/0067-0049/197/1/12](https://doi.org/10.1088/0067-0049/197/1/12)
- dos Santos, L. A., Meléndez, J., do Nascimento, J.-D., et al. 2016, *A&A*, 592, A156, doi: [10.1051/0004-6361/201628558](https://doi.org/10.1051/0004-6361/201628558)
- Dotter, A. 2016, *ApJS*, 222, 8, doi: [10.3847/0067-0049/222/1/8](https://doi.org/10.3847/0067-0049/222/1/8)
- Dransfield, G., Triaud, A. H. M. J., Guillot, T., et al. 2022, *MNRAS*, 515, 1328, doi: [10.1093/mnras/stac1383](https://doi.org/10.1093/mnras/stac1383)
- Eastman, J. 2017, EXOFASTv2: Generalized publication-quality exoplanet modeling code, *Astrophysics Source Code Library*. <http://ascl.net/1710.003>
- Eastman, J., Gaudi, B. S., & Agol, E. 2013, *PASP*, 125, 83, doi: [10.1086/669497](https://doi.org/10.1086/669497)
- Eastman, J. D., Rodriguez, J. E., Agol, E., et al. 2019, *arXiv e-prints*, arXiv:1907.09480. <https://arxiv.org/abs/1907.09480>
- Eberhardt, J., Hobson, M. J., Henning, T., et al. 2023, *AJ*, 166, 271, doi: [10.3847/1538-3881/ad06bc](https://doi.org/10.3847/1538-3881/ad06bc)
- Findeisen, K., Hillenbrand, L., & Soderblom, D. 2011, *AJ*, 142, 23, doi: [10.1088/0004-6256/142/1/23](https://doi.org/10.1088/0004-6256/142/1/23)
- Fortney, J. J., Marley, M. S., & Barnes, J. W. 2007, *ApJ*, 659, 1661, doi: [10.1086/512120](https://doi.org/10.1086/512120)
- Fortney, J. J., & Nettelmann, N. 2010, *SSRv*, 152, 423, doi: [10.1007/s11214-009-9582-x](https://doi.org/10.1007/s11214-009-9582-x)
- Gaia Collaboration, Vallenari, A., Brown, A. G. A., et al. 2023, *A&A*, 674, A1, doi: [10.1051/0004-6361/202243940](https://doi.org/10.1051/0004-6361/202243940)
- Gaudi, B. S., & Winn, J. N. 2007, *ApJ*, 655, 550, doi: [10.1086/509910](https://doi.org/10.1086/509910)
- Gill, S., Wheatley, P. J., Cooke, B. F., et al. 2020, *ApJL*, 898, L11, doi: [10.3847/2041-8213/ab9eb9](https://doi.org/10.3847/2041-8213/ab9eb9)
- Guillot, T., Abe, L., Agabi, A., et al. 2015, *Astronomische Nachrichten*, 336, 638, doi: [10.1002/asna.201512174](https://doi.org/10.1002/asna.201512174)
- Hansen, B. M. S., & Barman, T. 2007, *ApJ*, 671, 861, doi: [10.1086/523038](https://doi.org/10.1086/523038)
- Harris, C. R., Millman, K. J., van der Walt, S. J., et al. 2020, *Nature*, 585, 357, doi: [10.1038/s41586-020-2649-2](https://doi.org/10.1038/s41586-020-2649-2)
- Henry, G. W., Marcy, G. W., Butler, R. P., & Vogt, S. S. 2000, *ApJL*, 529, L41, doi: [10.1086/312458](https://doi.org/10.1086/312458)
- Hobson, M. J., Brahm, R., Jordán, A., et al. 2021, *AJ*, 161, 235, doi: [10.3847/1538-3881/abeaa1](https://doi.org/10.3847/1538-3881/abeaa1)

- Hobson, M. J., Trifonov, T., Henning, T., et al. 2023, *AJ*, 166, 201, doi: [10.3847/1538-3881/acfc1d](https://doi.org/10.3847/1538-3881/acfc1d)
- Jenkins, J. M., Twicken, J. D., McCauliff, S., et al. 2016, in Society of Photo-Optical Instrumentation Engineers (SPIE) Conference Series, Vol. 9913, Software and Cyberinfrastructure for Astronomy IV, ed. G. Chiozzi & J. C. Guzman, 99133E, doi: [10.1117/12.2233418](https://doi.org/10.1117/12.2233418)
- Jensen, E. 2013, Tapir: A web interface for transit/eclipse observability, Astrophysics Source Code Library. <http://ascl.net/1306.007>
- Johnson, M. C., Dai, F., Justesen, A. B., et al. 2018, *MNRAS*, 481, 596, doi: [10.1093/mnras/sty2238](https://doi.org/10.1093/mnras/sty2238)
- Jordán, A., Brahm, R., Espinoza, N., et al. 2019, *AJ*, 157, 100, doi: [10.3847/1538-3881/aafa79](https://doi.org/10.3847/1538-3881/aafa79)
- . 2020, *AJ*, 159, 145, doi: [10.3847/1538-3881/ab6f67](https://doi.org/10.3847/1538-3881/ab6f67)
- Kaufer, A., Stahl, O., Tubbesing, S., et al. 1999, *The Messenger*, 95, 8
- Kempton, E. M. R., Bean, J. L., Louie, D. R., et al. 2018, *PASP*, 130, 114401, doi: [10.1088/1538-3873/aadf6f](https://doi.org/10.1088/1538-3873/aadf6f)
- Kley, W., & Nelson, R. P. 2012, *ARA&A*, 50, 211, doi: [10.1146/annurev-astro-081811-125523](https://doi.org/10.1146/annurev-astro-081811-125523)
- Kurucz, R. L. 1992, in *IAU Symposium*, Vol. 149, The Stellar Populations of Galaxies, ed. B. Barbuy & A. Renzini, 225
- Lightkurve Collaboration, Cardoso, J. V. d. M., Hedges, C., et al. 2018, Lightkurve: Kepler and TESS time series analysis in Python, Astrophysics Source Code Library. <http://ascl.net/1812.013>
- Lindgren, L., Klioner, S. A., Hernández, J., et al. 2021, *A&A*, 649, A2, doi: [10.1051/0004-6361/202039709](https://doi.org/10.1051/0004-6361/202039709)
- Madhusudhan, N. 2019, *ARA&A*, 57, 617, doi: [10.1146/annurev-astro-081817-051846](https://doi.org/10.1146/annurev-astro-081817-051846)
- Madhusudhan, N., Amin, M. A., & Kennedy, G. M. 2014, *ApJL*, 794, L12, doi: [10.1088/2041-8205/794/1/L12](https://doi.org/10.1088/2041-8205/794/1/L12)
- Mamajek, E. E., & Hillenbrand, L. A. 2008, *ApJ*, 687, 1264, doi: [10.1086/591785](https://doi.org/10.1086/591785)
- Mayor, M., Pepe, F., Queloz, D., et al. 2003, *The Messenger*, 114, 20
- McCully, C., Volgenau, N. H., Harbeck, D.-R., et al. 2018, in Society of Photo-Optical Instrumentation Engineers (SPIE) Conference Series, Vol. 10707, Proc. SPIE, 107070K, doi: [10.1117/12.2314340](https://doi.org/10.1117/12.2314340)
- Mékarnia, D., Guillot, T., Rivet, J. P., et al. 2016, *MNRAS*, 463, 45, doi: [10.1093/mnras/stw1934](https://doi.org/10.1093/mnras/stw1934)
- Millholland, S. C., He, M. Y., & Zink, J. K. 2022, *AJ*, 164, 72, doi: [10.3847/1538-3881/ac7c67](https://doi.org/10.3847/1538-3881/ac7c67)
- Müller, S., & Helled, R. 2023, *Frontiers in Astronomy and Space Sciences*, 10, 1179000, doi: [10.3389/fspas.2023.1179000](https://doi.org/10.3389/fspas.2023.1179000)
- Nelson, R. P. 2018, in *Handbook of Exoplanets*, ed. H. J. Deeg & J. A. Belmonte, 139, doi: [10.1007/978-3-319-55333-7\\_139](https://doi.org/10.1007/978-3-319-55333-7_139)
- Pecaut, M. J., & Mamajek, E. E. 2013, *ApJS*, 208, 9, doi: [10.1088/0067-0049/208/1/9](https://doi.org/10.1088/0067-0049/208/1/9)
- Pepe, F., Mayor, M., Galland, F., et al. 2002, *A&A*, 388, 632, doi: [10.1051/0004-6361:20020433](https://doi.org/10.1051/0004-6361:20020433)
- Pepper, J., Pogge, R. W., DePoy, D. L., et al. 2007, *PASP*, 119, 923, doi: [10.1086/521836](https://doi.org/10.1086/521836)
- Petigura, E. A., Sinukoff, E., Lopez, E. D., et al. 2017, *AJ*, 153, 142, doi: [10.3847/1538-3881/aa5ea5](https://doi.org/10.3847/1538-3881/aa5ea5)
- Pollacco, D. L., Skillen, I., Collier Cameron, A., et al. 2006, *PASP*, 118, 1407, doi: [10.1086/508556](https://doi.org/10.1086/508556)
- Queloz, D., Mayor, M., Udry, S., et al. 2001, *The Messenger*, 105, 1
- Ricker, G. R., Winn, J. N., Vanderspek, R., et al. 2015, *Journal of Astronomical Telescopes, Instruments, and Systems*, 1, 014003, doi: [10.1117/1.JATIS.1.1.014003](https://doi.org/10.1117/1.JATIS.1.1.014003)
- Schlecker, M., Kossakowski, D., Brahm, R., et al. 2020, *AJ*, 160, 275, doi: [10.3847/1538-3881/abbe03](https://doi.org/10.3847/1538-3881/abbe03)
- Schlegel, D. J., Finkbeiner, D. P., & Davis, M. 1998, *ApJ*, 500, 525, doi: [10.1086/305772](https://doi.org/10.1086/305772)
- Schmider, F.-X., Abe, L., Agabi, A., et al. 2022, in Society of Photo-Optical Instrumentation Engineers (SPIE) Conference Series, Vol. 12182, Ground-based and Airborne Telescopes IX, ed. H. K. Marshall, J. Spyromilio, & T. Usuda, 121822O, doi: [10.1117/12.2628952](https://doi.org/10.1117/12.2628952)
- Schulte, J., Rodriguez, J. E., Bieryla, A., et al. 2024, *AJ*, 168, 32, doi: [10.3847/1538-3881/ad4a57](https://doi.org/10.3847/1538-3881/ad4a57)
- Smith, J. C., Stumpe, M. C., Van Cleve, J. E., et al. 2012, *PASP*, 124, 1000, doi: [10.1086/667697](https://doi.org/10.1086/667697)
- Stassun, K. G., Oelkers, R. J., Paegert, M., et al. 2019, *AJ*, 158, 138, doi: [10.3847/1538-3881/ab3467](https://doi.org/10.3847/1538-3881/ab3467)
- Stumpe, M. C., Smith, J. C., Catanzarite, J. H., et al. 2014, *PASP*, 126, 100, doi: [10.1086/674989](https://doi.org/10.1086/674989)
- Stumpe, M. C., Smith, J. C., Van Cleve, J. E., et al. 2012, *PASP*, 124, 985, doi: [10.1086/667698](https://doi.org/10.1086/667698)
- Thorngren, D. P., Fortney, J. J., Murray-Clay, R. A., & Lopez, E. D. 2016, *ApJ*, 831, 64, doi: [10.3847/0004-637X/831/1/64](https://doi.org/10.3847/0004-637X/831/1/64)
- Tokovinin, A. 2018, *PASP*, 130, 035002, doi: [10.1088/1538-3873/aaa7d9](https://doi.org/10.1088/1538-3873/aaa7d9)
- Tokovinin, A., Fischer, D. A., Bonati, M., et al. 2013, *PASP*, 125, 1336, doi: [10.1086/674012](https://doi.org/10.1086/674012)
- Trifonov, T., Brahm, R., Espinoza, N., et al. 2021, *AJ*, 162, 283, doi: [10.3847/1538-3881/ac1bbe](https://doi.org/10.3847/1538-3881/ac1bbe)
- Trifonov, T., Brahm, R., Jordán, A., et al. 2023, *AJ*, 165, 179, doi: [10.3847/1538-3881/acba9b](https://doi.org/10.3847/1538-3881/acba9b)
- Udry, S., Mayor, M., Naef, D., et al. 2000, *A&A*, 356, 590

- Van Eylen, V., Dai, F., Mathur, S., et al. 2018, MNRAS, 478, 4866, doi: [10.1093/mnras/sty1390](https://doi.org/10.1093/mnras/sty1390)
- Vanderburg, A., & Johnson, J. A. 2014, PASP, 126, 948, doi: [10.1086/678764](https://doi.org/10.1086/678764)
- Winn, J. N., & Fabrycky, D. C. 2015, ARA&A, 53, 409, doi: [10.1146/annurev-astro-082214-122246](https://doi.org/10.1146/annurev-astro-082214-122246)
- Zacharias, N., Finch, C., & Frouard, J. 2017, VizieR Online Data Catalog, 1340
- Zhou, G., Rodriguez, J. E., Collins, K. A., et al. 2016, AJ, 152, 136, doi: [10.3847/0004-6256/152/5/136](https://doi.org/10.3847/0004-6256/152/5/136)
- Ziegler, C., Tokovinin, A., Briceno, C., et al. 2019, arXiv e-prints, arXiv:1908.10871.  
<https://arxiv.org/abs/1908.10871>